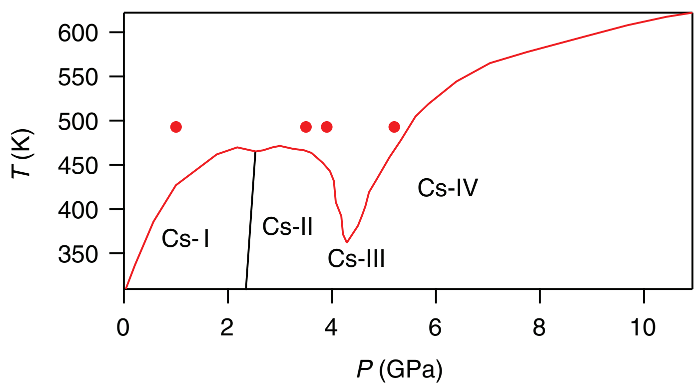

Figure 5.1. Phase diagram of Cs from Ref. [12] in the pressure and temperature region of interest here. Full circles correspond to the experimental points investigated in the liquid: 1, 3.5, 3.9, and 5.2 GPa at 493 K.

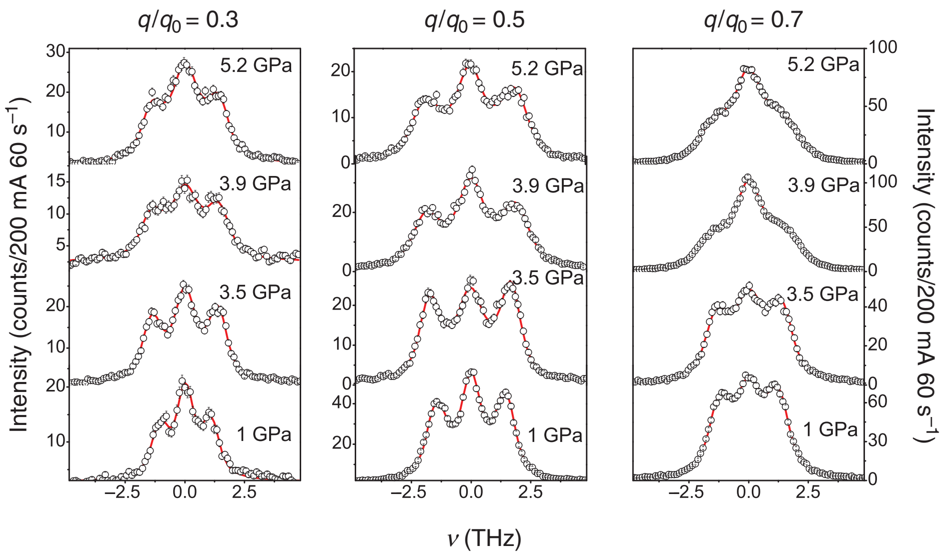

Figure 5.2. Experimental spectra for the four investigated pressure points are reported at similar q/q_0 values, indicated on the top of the figure, together with the best fit using Eqs. 1–3. The experimental error corresponds to the symbol size.

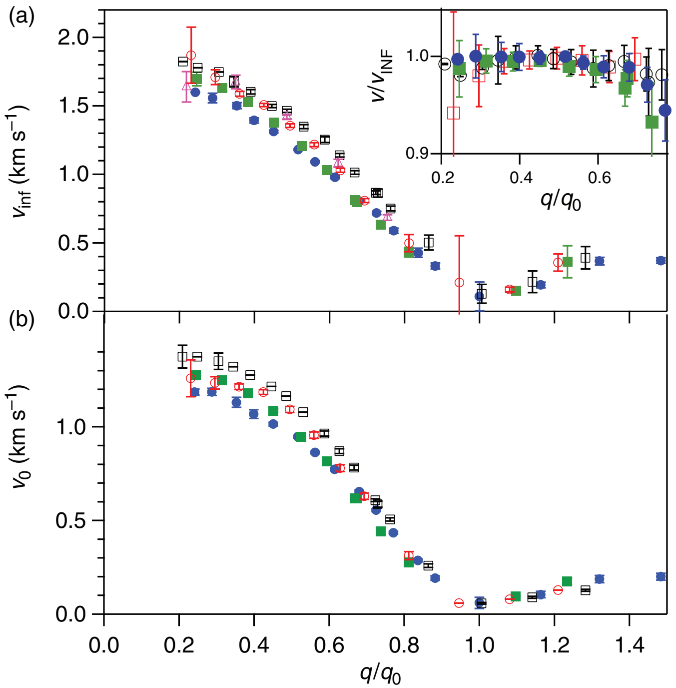

Figure 5.3. Infinite-frequency (**a**) and zero-frequency (**b**) sound velocity as obtained from the viscoelastic fit, for liquid Cs at 1 GPa (blue full circles), 3.5 GPa (green full squares), 3.9 GPa (black empty squares), and 5.2 GPa (red empty circles). The inset in the panel (**a**) shows the ratio of the apparent sound velocity to the infinite frequency limit, same symbols as in the main panel. Up to $q/q_0 = 0.6$, the liquid is at its elastic limit at all pressures.

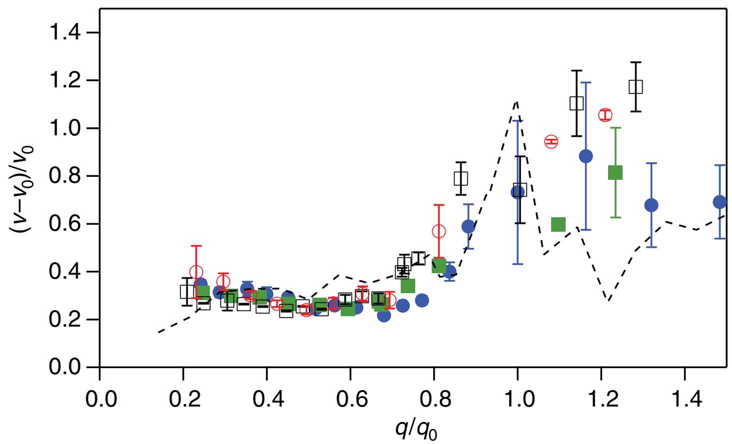

Figure 5.4. The positive dispersion of the sound velocity, measured as $(v - v_0)/v_0$, is reported at all the investigated pressures, same symbols as in Fig. 3. Remarkably, it does not depend on pressure. Data from Ref. [16] at the room pressure melting point, 308 K, are also reported (dashed line).

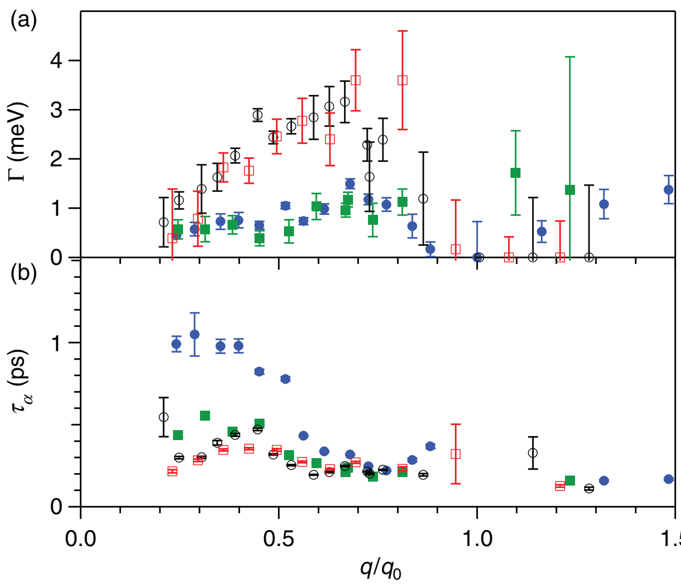

Figure 5.5. The microscopic relaxation parameter Γ (**a**) and the structural relaxation time τ_α (**b**) derived from the viscoelastic fit, same symbols as in Fig. 3. While τ_α decreases gradually with pressure, Γ shows a discontinuous increase at the transition to more than twice of the low-pressure value.

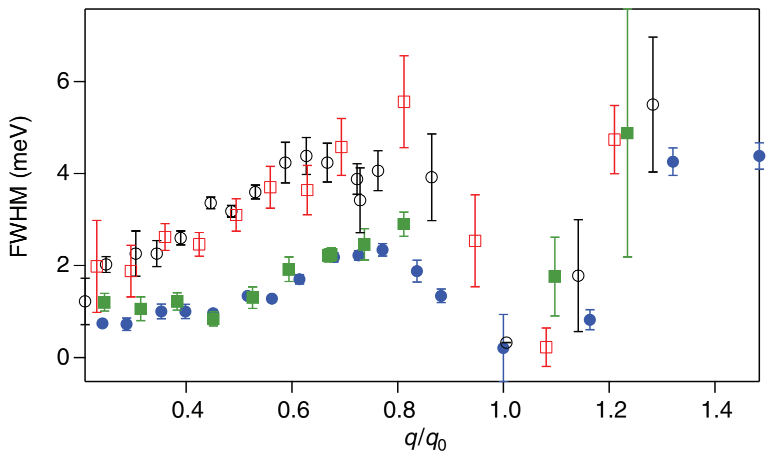

Figure 5.6. The width of the inelastic peaks of the longitudinal current is reported as a function of q/q_0, same symbols as in Fig. 3. The FWHM values are density independent in each of the two liquid phases and show a discontinuous jump at the transition.